Evaluation of an Electrodeposited Bimetallic Cu/Ag Nanostructured Screen Printed Electrode for Electrochemical Surface-Enhanced Raman Spectroscopy (EC-SERS) Investigations

JES Focus Issue on Biosensors and Micro-Nano Fabricated Electromechanical Systems

Evaluation of an Electrodeposited Bimetallic Cu/Ag Nanostructured Screen Printed Electrode for Electrochemical Surface-Enhanced Raman Spectroscopy (EC-SERS) Investigations

O. J. R. Clarke, G. J. H. St. Marie, and C. L. Brosseau*,z

Department of Chemistry, Saint Mary's University, Halifax, Nova Scotia, Canada

The field of plasmonics has experienced rapid growth over the past decade with a host of emerging applications including single molecule sensing and plasmon-assisted catalysis. The vast majority of these applications use either silver or gold as the plasmonic metal, which are both high cost and face earth-abundance limitations in the next 100 years. Recent efforts have focused on taking advantage of the plasmonic properties of copper, a more abundant and low cost coinage metal as a sustainable route for plasmonic applications. In particular, there has been great interest in developing copper substrates capable of reliable and efficient enhancement of Raman signals for use in surface-enhanced Raman spectroscopy (SERS) sensing. Herein we describe a sequential electrodeposition technique whereby highly functional and robust Cu/Ag bimetallic SERS-active screen printed electrodes can be produced rapidly and at low cost, which display excellent plasmonic performance and are capable of supporting surface-plasmon assisted catalysis (SPAC). This modified screen printed electrode allows for the in situ spectroelectrochemical investigation of surface redox processes using a sustainable alternative to traditional monometallic electrodes.

Manuscript submitted October 12, 2016; revised manuscript received December 29, 2016. Published February 11, 2017. *This paper is part of the JES Focus Issue on Biosensors and Micro-Nano Fabricated Electromechanical Systems.*

Over the past several decades there has been growing interest in the field of plasmonics, in particular due to the many applications which are possible now, and may be possible in the future with such a technology. In particular, SERS-based sensing, which relies heavily on the localized surface plasmon resonance (LSPR) to contribute to the large enhancement in signal, has shown promise for a multitude of applications ranging from medical diagnostics to art conservation to environmental monitoring.[1–5] While Ag and Au form the bulk of metals used for SERS-based sensing, there is growing interest in the use of Cu as a plasmonic substrate due to its relatively low cost and high earth abundance.[6–8] In particular, large scale applications of plasmonics such as in plasmon-enhanced photovoltaics are going to require exploration of more readily scalable metals such as Cu.[9]

Cu-based SERS substrates were first explored in the early 1980's, but recent progress in this area has been slow. Limitations with the use of Cu for SERS-based sensing extend from two main issues – the ease of oxidation of Cu, which leads to a dampening of the plasmon resonance, as well as a lack of reported stable nanostructures.[10] In addition, as with Au, Cu cannot be used for plasmonic applications below ~600 nm due to interfering interband transitions.[10] That being said, in recent years several groups have been working to realize the possibility of Cu-based SERS. For example, Chen et al. reported a highly efficient nanoporous Cu SERS substrate produced by de-alloying of a $Cu_{30}Mn_{70}$ alloy.[11] In this case, selective etching of the Mn resulted in Cu nanopores with tunable sizes. In 2014, Bassetto et al. evaluated a copper-based sphere segment void (SSV) SERS structure produced using a combination of nanosphere lithography and electrochemical deposition. In this way, the authors reported a robust Cu-based SERS active electrode which provided good quality spectra for the amino acids tryptophan and serine.[12] More recently, Yang et al. demonstrated that a self-seeded growth approach could be used to produce five-fold twinned copper nanowires, resulting in efficient SERS enhancement for 4-mercaptobenzoic acid.[13] Despite examples such as these, truly high quality Cu-based SERS substrates remain to a large extent elusive.

In order to take advantage of the low cost and great abundance of copper, while retaining the excellent plasmonic performance afforded by Au and Ag, along with their improved stability, recent reports have investigated the possibility of combining these metals. Such bimetallic and multimetallic SERS substrates have indeed shown promise for next generation sensing. Toshima et al. reported the first copper bimetallic SERS substrate (Cu/Pd) in 1999, where the nanometer-sized Au/Pd colloidal particles were synthesized using a polyol reduction method.[14] More recent reports have focused on Cu/Ag bimetallic structures for SERS sensing, produced using a variety of techniques including laser-assisted Galvanic replacement,[15] AAO template-assisted approaches[16] and electrodeposition.[17]

In this work, we seek to extend the use of the Cu/Ag bimetallic system for SERS based sensing through the development of a fast and cost-effective route for bimetallic deposition using sequential electrodeposition onto readily available carbon-based screen printed electrodes. Sequential electrodeposition of first Cu, followed by Ag, allows for the deposition of regular flower-like Ag nanostructures onto uniformly sized Cu microcubes. These new electrochemical-SERS (EC-SERS) substrates are then compared to traditional silver-only substrates, where a clear advantage of the bimetallic substrate is illustrated at 785 nm excitation, not only in terms of signal enhancement and quality, but also in terms of the reduction of the amount of Ag required.

Experimental

Reagents, solutions and electrode materials.—Copper (II) nitrate hydrate (99.999% $Cu(NO_3)_2 \bullet H_2O$), silver nitrate (99.9999% $AgNO_3$), and sodium fluoride (99.99%, NaF) were all purchased from Sigma-Aldrich (St. Louis, MO, USA). Sodium citrate dihydrate (≥99%, $Na_3C_6H_5O_7 \bullet 2H_2O$) and sodium borohydride (≥99%, $NaBH_4$) were purchased from Fluka (Buchs, Switzerland). All glassware for this research was cleaned by immersion in neat sulfuric acid overnight, followed by careful rinsing with Millipore water (>18.2 MΩ•cm). All solutions were prepared using Millipore water as well. The carbon screen printed electrodes (SPE) (15 mm × 61 mm × 0.36 mm) were purchased from Pine Research Instrumentation (Durham, NC, USA) and consisted of a silver/silver chloride (Ag/AgCl) reference electrode, a carbon counter electrode, and a carbon working electrode. All reagents were used without further purification.

Electrochemical and spectroscopic instrumentation.—For the electrodeposition, a Princton Applied Research Model 273A

*Electrochemical Society Member.
zE-mail: christa.brosseau@smu.ca

potentiostat was utilized, and PowerSuite software was used to set the electrodeposition parameters. For the Raman spectroscopy, two different Raman instruments were used throughout this project. The majority of the experiments were conducted using a DeltaNu benchtop Raman spectrometer equipped with a 785 nm laser (Intevac Photonics, Santa Clara, USA). The spectrometer resolution is 5 cm^{-1} and it is equipped with an air-cooled CCD detector, an optics extension tube, and a right angle optics attachment. Sample acquisition times ranged from 30–60 seconds at laser powers ranging between 22.3–55.9 mW. For some experiments a DXR Smart Raman spectrometer equipped with 532 nm laser (Thermo Fisher Scientific, Mississauga, ON, Canada) was utilized. The spectrometer resolution is 3 cm^{-1} and it also is equipped with an air-cooled CCD detector. The laser power used in this case was 3 mW. All Raman data are corrected for both laser power and acquisition time. Origin 8.1 was used for the spectral processing and data analysis (OriginLab Corporation, Northampton, MA, USA). For the EC-SERS studies, both Raman spectrometers were coupled to a Pine Research Instrumentation portable USB Wavenow potentiostat/galvanostat (Durham, NC, USA). For EC-SERS, a deaerated 0.1 M NaF solution was used as the supporting electrolyte, and the applied potential ranged from 0.0 V to −1.0 V vs Ag/AgCl in increments of 0.1 V for a time interval of 60 seconds. All potentials are reported vs. Ag/AgCl unless otherwise stated.

Preparation of Cu/Ag bimetallic screen printed electrodes via sequential electrodeposition.—In this work, we build upon our expertise in developing SERS-active screen printed electrodes for rapid sensing of target analytes using electrochemical SERS (EC-SERS), as was highlighted in our previous work.[18a,18b] For the present study, bimetallic Cu/Ag nanostructured screen printed electrodes were obtained by first preparing a 0.1 M solution of copper (II) nitrate and a 1.0×10^{-4} M silver nitrate solution. The copper (II) nitrate solution was first purged under a stream of argon for 15–20 minutes. 10.0 mL of the deaerated copper nitrate solution was then measured into a glass vial and purged with argon for a further 5 minutes. The solution was stirred using a magnetic stirrer (180 rpm), and the copper was then electrodeposited from the 0.1 M $Cu(NO_3)_2$ solution by holding the potential at −0.300 V vs Ag/AgCl for 180.0 seconds. Once the electrodeposition of the copper was complete, varying amounts of the deaerated 1.0×10^{-4} M $AgNO_3$ were added to the electrochemical cell containing the $Cu(NO_3)_2$, the solution was stirred and the electrodeposition was repeated (−0.300 V, 180.0 seconds). Once the electrodeposition of the silver was complete, the electrode was removed and rinsed with deionized water and left to dry in air for 30 minutes prior to measurement. This sequential electrodeposition was only performed once to obtain the desired material, as is illustrated in Figure S-1.

Preparation of modified Lee-Meisel silver nanoparticles.—Traditional silver nanoparticles prepared via a modified Lee-Meisel synthesis, and reported previously,[18a,18b] were prepared for the sake of comparison in the present study. Briefly, 95 mL of deionized water was poured into a three-necked round bottom flask followed by 1.0 mL of 0.1 M silver nitrate solution, 3.4 mL of 5% sodium citrate and 0.6 mL of 0.17 M citric acid. The reflux condenser was connected to the three-necked round bottom flask which was covered in foil. The solution was then stirred and 0.2 mL of 1×10^{-4} M sodium borohydride was added to the solution. The solution was then heated at 225°C for 20 minutes and left to cool while stirring for one hour. The bulk solution was transferred to 1.5 mL Eppendorf tubes and centrifuged twice at 8000 rpm for 20 minutes and the supernatant was removed each time. 3×5 µL of the concentrated colloidal sol was drop-coated onto the screen printed electrode (SPE) (each layer was allowed to dry completely prior to addition of the next layers) and the electrode was then left to dry in air for an hour prior to measurement.

Characterization.—In order to evaluate the structure and chemical nature of the electrodeposited structures in this work, a TESCAN Mira3 LMU field emission scanning electron microscope (FE-SEM), equipped with an Oxford X-Max 80 mm^2 SDD energy-dispersive x-ray (EDX) detector was utilized. ImageJ software (National Institutes of Health, Bethesda, Maryland, USA) was used for image analysis where appropriate.[19]

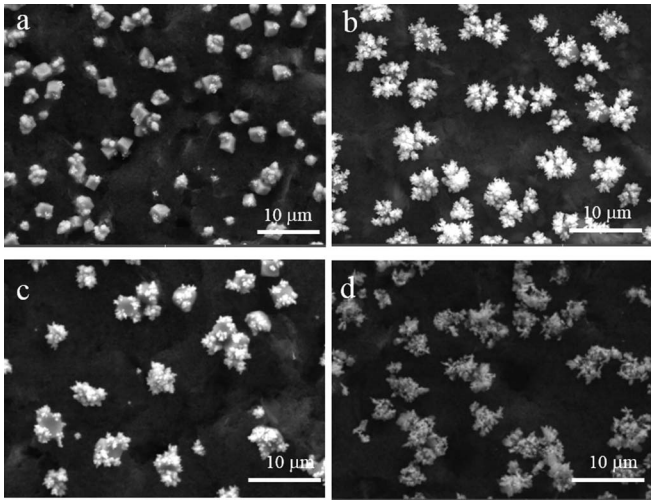

Figure 1. FE-SEM images of sequentially electrodeposited Cu/Ag bimetallic structures obtained with the following amounts of 0.1 mM $AgNO_3$, added to the copper nitrate solution after the Cu electrodeposition step: (a) 250 µL (b) 500 µL (c) 750 µL and (d) 1000 µL.

Results and Discussion

Characterization of electrodeposited bimetallic Cu/Ag structures.—Figure 1 shows the FE-SEM images for the screen printed electrode after the sequential electrodeposition as described above, where 250, 500, 750 and 1000 µL of 1.0×10^{-4} M $AgNO_3$ were added to the $Cu(NO_3)_2$ solution for the second electrodeposition step. Figure 2a shows a zoomed-in image of Figure 1a, showing the formation of silver-decorated copper cubes; the cubes were observed to be both complete and tip-truncated. Figure 2b shows the EDX spectrum for a bare edge of one of the cubic structures, indicating that the cubic structures are indeed copper, with some amount of

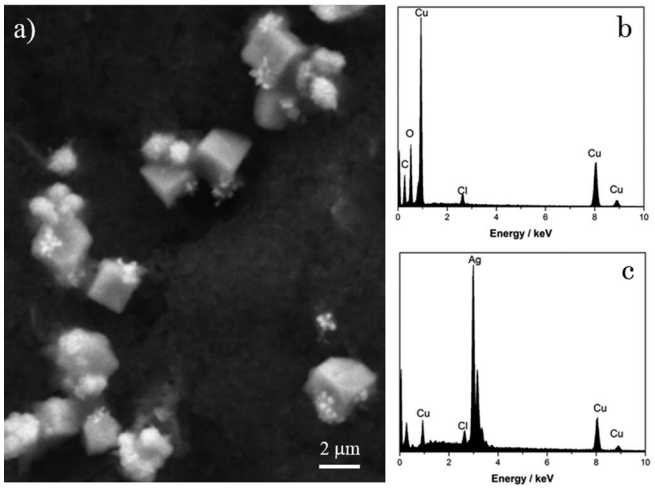

Figure 2. (a) FE-SEM of the electrodeposited structure obtained when 250 µL of 1.0×10^{-4} M $AgNO_3$ is added to the copper nitrate solution after the Cu electrodeposition step. (b) EDX spectrum for a bare face of one of the cubic structures shown in Figure 2a (c) EDX spectrum for one of the decorated edges of the cubic structures shown in Figure 2a.

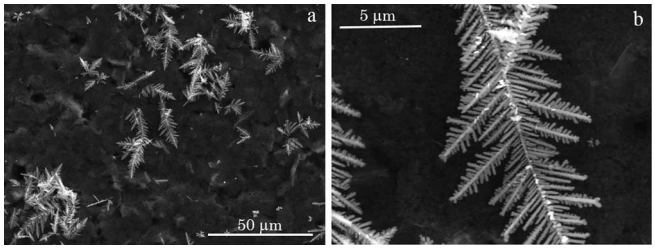

Figure 3. FE-SEM images of the electrodeposition product formed when Cu^{2+} and Ag^{+} are both present in solution, as opposed to the sequential electrodeposition shown in Figures 1 and 2. EDX analysis confirmed all electrodeposited solid was silver.

oxidation. Since oxygen is always present in the vacuum chamber of the FE-SEM to some extent, one is unable to quantify the amount of copper oxidation using this technique. Since no precautions were taken to protect the copper surface from oxidation prior to imaging, partial oxidation would be expected for these structures. Figure 2c is the EDX spectrum for one of the decorated edges, showing that the flower-like decoration on the cubic structure is indeed silver. From these two figures, several key findings are evident: firstly, as the concentration of Ag^{+} increases, the amount of flower-like decoration on the underlying cubic copper structures increases. Secondly, deposition of the metallic silver occurs primarily on the copper structures, with little deposition on the underlying carbon electrode. The 500 μL addition of the 1.0×10^{-4} M $AgNO_3$ (Figure 1b) was found to give the most densely packed and uniform Ag nanoflowers as well as the strongest and most uniform SERS signal, and as such this condition was used for the remainder of this work. A higher resolution image of the structures present in Figure 1b can be found in the supporting information (Figure S-2). It was noted that most of the silver deposits formed first at either a face or an edge of the copper cube. This is likely due to the fact that copper oxide cubic structures are known to have faces which are [100] facets, which are slightly negatively charged, with truncated [111] corners, which are slightly positively charged. Thus, the more negatively charged facet should attract the positively charged silver ion preferentially.[20] In addition, edges are known to be highly reactive and thus also a likely site for initiation of deposition.

Interestingly, when the copper and silver solutions were mixed prior to the copper electrodeposition step, both metals deposited as monometallic structures during electrodeposition, with silver being the dominant deposit. In addition, the electrodeposited silver structure was the typical fern-like, dendritic structure observed for Galvanic deposition of silver, which is known to have poorly controlled growth characteristics. A FE-SEM of this is shown in Figure 3.

Electrodeposition of both Cu^{2+} and Ag^{+} is common in the literature. Ag^{+} has a more positive standard reduction potential of +0.799 V vs SHE (Ag^{+}/Ag^{0}) compared to Cu^{2+} (+0.337 V vs SHE, Cu^{2+}/Cu^{0}).[21] As a result, reduction of Ag^{+} is more favorable than Cu^{2+}. When these two ions are both present in solution under the electrodeposition conditions used in this work, Ag will electrodeposit first. The dendritic structures observed in Figure 3 are very commonly observed for electrodeposited silver, even when various anions and cations are introduced into the electrolyte. This dendritic growth is believed to occur via a diffusion-limited growth model wherein growth of the deposit occurs in a nucleation-adsorption-growth-branching process.[22] Such Ag nanodendrite (AgND) substrates have been extensively studied as potential SERS substrates. For example, Wang et al. reported a controlled electrodeposition method for fabricating AgNDs on a microwell-patterned electrode.[23] In this case, the authors were able to demonstrate highly enhanced SERS activity for rhodamine 6G. Li et al. demonstrated a SERS-active AgND-coated Ag core-shell hierarchical microsheet structure fabricated through electrodeposition; in this case efficient SERS activity for rhodamine 6G was again demonstrated.[24] More recently, Zhang et al. showed that AgND could be electrodeposited onto the surface and embedded into the channels of a porous anodic aluminum oxide (AAO) template, demonstrating a 3-D SERS substrate capable of detecting rhodamine 6G down to 10^{-11} M.[25] Despite the potential that AgND structures offer for SERS based sensor development, significant challenges remain, including stability of the delicate nanodendrites, signal inhomogeneity and the high-cost and earth abundance limitations associated with the use of pure Ag.

In the present work, copper microstructures were electrodeposited first, followed by electrodeposition of Ag. While Galvanic (spontaneous) deposition of Ag will occur in the presence of Cu(s), in this case electrodeposition will facilitate a faster and more controlled deposition onto the copper microcube structures. In contrast to the Ag nanodendrite structure highlighted above, the hierarchical silver nanostructure observed under these electrodeposition conditions is more flower-like and less dendritic. For reference, a control study was undertaken wherein the first copper electrodeposition step was completed, and afterwards the silver nitrate was added to the electrolyte. However, in this case the second electrodeposition step was not completed, but rather Galvanic replacement of copper with silver was allowed to take place for an equivalent amount of time. The FE-SEM of the resultant substrate is shown in the supporting information in Figure S-3. In this case, the silver deposit is clearly needle-like and very inhomogeneous, and the flower-like structures are not observed under these conditions.

Nanoflower-like Ag structures have been reported by Bian et al. when silver was electrodeposited onto ITO-coated glass. Of particular note was the relatively low polydispersity reported for these nanoflowers, which were composed of quasi-spherical particles with a preference for the fcc Ag(111) orientation. SERS detection was possible for rhodamine 6G down to 10^{-10} M for these substrates.[26,27] Finite difference time domain (FDTD) calculations as well as experimental data reported by Fang et al. demonstrated that such Ag flower-like structures have an exceedingly high abundance of SERS-active hot spots, which leads to excellent sensitivity, with enhancement factors in excess of 10^{7}.[28]

Despite the great interest in electrodeposited Ag substrates for SERS applications, relatively little work has been done in the area of bimetallic Cu/Ag SERS substrates produced through electrodeposition. In 2012, Ke et al. published work on the fabrication of SERS arrays via Galvanic replacement of silver onto electrochemically deposited copper micro-patterned substrates. In this case, copper was electrodeposited onto a microcontact-printed gold film, after which the Cu-patterned substrates were immersed into a $AgNO_3$ solution whereby Galvanic replacement of the Cu for Ag was allowed to occur.[29] In this case, decent SERS spectra were recorded for both rhodamine 6G and p-ATP, with an estimated enhancement factor of $\sim 10^{6}$. More recently, Li et al. reported a facile electrodeposition method for bimetallic Cu/Ag structures on graphene paper.[30] In this work, a co-electrodeposition method was used, and at high applied voltages for extended periods of time, Cu/Ag bimetallic dendritic structures were deposited onto graphene. However, it was noted that the two metals deposited as distinctive phases and no true alloy was formed. Efficient SERS was demonstrated for 4-MBA, with a reported enhancement factor of $\sim 10^{5}$. In this case, a synergistic effect between the copper and silver nanostructures was credited with improving the electromagnetic enhancement for SERS.

In the present work, sequential electrodeposition is reported for the first time as a facile method for the creation of bimetallic Cu/Ag structures onto a carbon-based screen printed electrode (SPE) for use in electrochemical-SERS (EC-SERS) investigations. The combination of the uniform cubic copper microstructures and the hierarchical Ag nanoflowers was anticipated to provide excellent SERS enhancement for EC-SERS.

SERS for bimetallic Cu/Ag SPE compared to Ag only SPE.—In the next part of this work, the SERS enhancement for the Cu/Ag SPE was assessed. For this step, 10.0 μL of 1.0 mM *para*-aminothiophenol (p-ATP) was drop-coated onto the surface of the modified SPE and

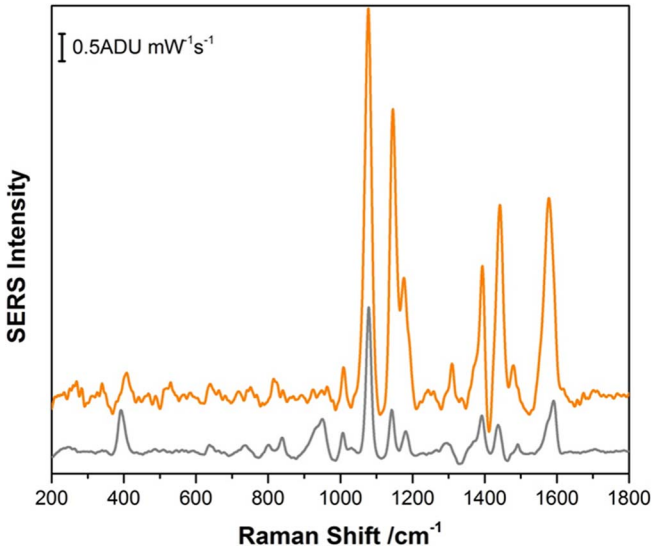

Figure 4. SERS of 1.0 mM p-ATP on bimetallic Cu/Ag SPE (orange spectrum) and AgNP SPE (gray spectrum) measured at 785 nm excitation, 30 second acquisition, 22.3 mW.

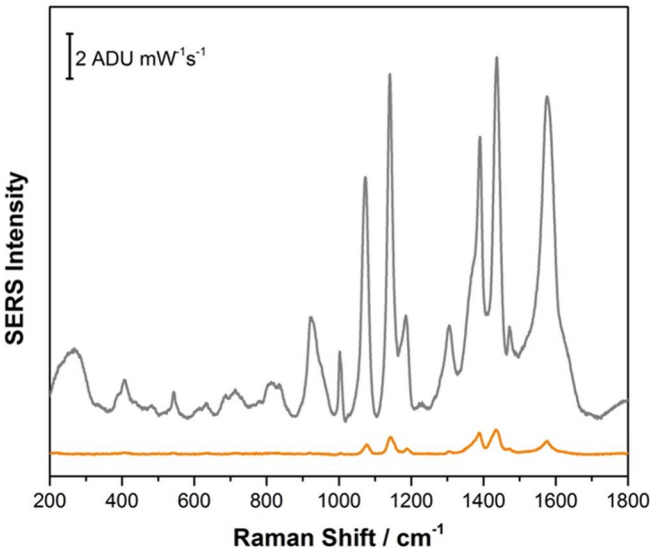

Figure 5. SERS of 1.0 mM p-ATP on bimetallic Cu/Ag SPE (orange spectrum) and AgNP SPE (gray spectrum) measured at 532 nm excitation, 30 second acquisition, 3 mW.

the electrode was allowed to dry. Figure 4 shows the comparison of the SERS signal at 785 nm in air for the Cu/Ag SPE and for a SPE coated with the modified Lee-Meisel Ag colloids only. Clearly there is a significant enhancement in the SERS signal upon moving to the bimetallic Cu/Ag system, with a greater than 5-fold increase in signal observed. As the modified Lee-Meisel AgNPs have previously been reported by us to have an enhancement factor of $\sim 10^8$, we anticipate the current bimetallic Cu/Ag SERS substrate therefore has an enhancement factor in excess of 10^8.[31] Others have similarly reported strengthened surface plasmon resonances in Cu/Ag bimetallic nanostructures, likely a result of strong near-field coupling between the two metals.[32] Sharma et al. noted that when present in alloy form, bimetallic nanoparticles are capable of simultaneously providing enhanced sensitivity, improved signal-to-noise ratios and extended operating ranges when compared to single metal nanoparticle systems.[33] In addition, Zamkovets et al. reported enhanced plasmon resonances in bimetallic Cu-Ag structures due to differential electronegativites in the two metals, which allows the silver to pull electron density from the copper metal.[34] Important to mention is the significant reduction in silver required for the Cu/Ag electrode; while the Lee-Meisel preparation requires 1.0×10^{-4} mol of Ag^+, the Cu/Ag electrodeposition requires only 5.0×10^{-8} mol of Ag^+, representing a 2000X decrease in the amount of required metal cation. Also interesting to note is the relatively good spot-to-spot SERS signal reproducibility obtained for the Cu/Ag substrate, as shown in Figure S-4.

Interestingly, when the SERS comparison was made for the two modified SPEs, but this time at an excitation wavelength of 532 nm (Figure 5), the SPE modified with pure silver was the most efficient for SERS, with the SERS effect for the bimetallic Cu/Ag exhibiting marked dampening of the plasmonic response. This is interesting as it suggests that the interplay between the copper and silver in terms of enhancing the electromagnetic effect is strongly influenced by the incident radiation wavelength. In this case it is entirely likely that interband transitions present in the copper are attenuating the SERS response for the bimetallic system.

Electrochemical SERS of p-ATP using bimetallic Cu/Ag SPE.— The next stage of this project was to assess the utility of this new bimetallic Cu/Ag SPE for routine spectroelectochemistry. In this case, the p-ATP was again added to the SERS substrate as described in the previous section and allowed to air-dry. Next, the SPE was placed into the spectroelectrochemical cell containing 0.1 M NaF (deaerated) as supporting electrolyte, and EC-SERS data were collected as a function of applied potential from 0.0 V to −1.0 V in 100.0 mV increments. Figure 6 shows the EC-SERS spectra for both the cathodic and anodic stepping sequences. At open circuit potential (OCP), prior to the application of a voltage, the SERS signal for the monolayer of p-ATP is strong, and the signal strength increases in intensity until about −0.2 V vs Ag/AgCl, at which point the signal intensity decreases. At −0.8 V, the SERS signal has mostly disappeared. Upon returning to less negative potentials, the SERS signal for p-ATP is observed to increase considerably, such that at open circuit potential *after* the application of the voltage, the p-ATP signal is ∼4 times larger than it originally was. These results illustrate the power of EC-SERS not only for evaluating redox phenomena but also for increasing the sensitivity possible for SERS in general. Also of note are the peaks at 1141, 1390 and 1443 cm^{-1}, which are due to the formation of the plasmon-assisted catalytic product 4,4'-dimercaptoazobenzene (DMAB) on the surface.[35,36] These peaks are originally present at OCP, and grow in intensity until about −0.2 V, after which the intensity begins to decrease. This signal reduction is due to the electrochemical reduction of the DMAB product back to p-ATP. Upon electrochemical re-oxidation of p-ATP to DMAB, the SERS signal increases dramatically, especially for the three peaks assigned to DMAB in particular. While the extreme potential dependence observed for the SERS signal in this case is dramatic, the reason behind this is difficult to explain. Osawa et al. studied this system in 1994, and attributed the potential dependence not to molecular adsorption/desorption or surface reorientation of p-ATP, but rather to a manifestation of the chemical enhancement mechanism in SERS.[37] In this case, the EC-SERS signal for p-ATP was recorded on a silver thin-film electrode at two different excitation wavelengths, and the potential dependence of the SERS signal was found to depend strongly on the energy of the incident radiation. It should be noted however, that this conclusion was based on assigning the 1442 cm^{-1} mode to p-ATP rather than to DMAB, which is now believed to be incorrect.[35,36] Since the three peaks attributed to DMAB display the largest dependence on potential as highlighted in the present work, this is an indication that the plasmon-assisted catalysis is in fact what is most strongly driven by any potential charge-transfer contributions facilitated through manipulation of the Fermi level of the metal electrode. In addition, it is very possible that p-ATP and DMAB have different surface orientation preferences, which is reflected in the potential-dependent changes in signal intensity, a result of the surface selection rules at play in SERS. While many questions about this system remain to be answered, this study

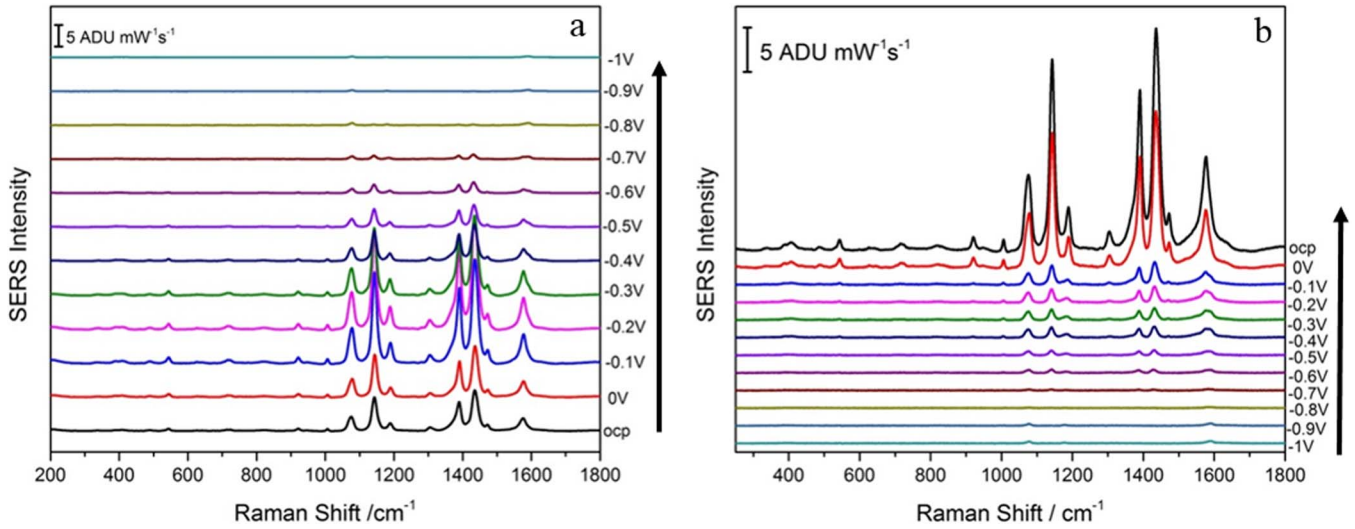

Figure 6. EC-SERS data collected using the bimetallic Cu/Ag SPE at 785 nm excitation, 30 second acquisition and 22.3 mW laser power at the sample. (a) Cathodic sequence (b) Anodic sequence. Arrows indicate direction of potential stepping.

is an excellent example of how EC-SERS can be utilized to follow a surface redox process in-situ at an electrified interface.

In summary, a facile method for the fabrication of cost-effective, robust and sustainable SERS-active electrodes has been highlighted in this work for the first time on commercially available screen printed electrodes. Coupling of these more sustainable substrates with portable potentiostats and bench-top spectrometers allows for rapid access to valuable spectroelectrochemical data; this data can be further utilized for a vast array of applications ranging from rapid and sensitive SERS-based biosensing to a deeper understanding of surface-plasmon assisted catalysis, which offers an entirely new route for heterogeneous catalysis.

Conclusions

This work demonstrates the first use of sequential electrodeposition for the facile creation of SERS-active bimetallic Cu/Ag hierarchical structures directly onto carbon-based screen printed electrodes. As a result, high performance, low-cost SERS-active electrodes were created using a minimal amount of the earth-limited Ag metal. This new EC-SERS electrode was used to study the plasmon-assisted catalytic conversion of p-ATP to DMAB in-situ, spectroelectrochemically. At 785 nm excitation, this bimetallic Cu/Ag electrode was shown to be superior in performance to a monometallic Ag SPE, thus representing a more sustainable alternative for future EC-SERS investigations.

Acknowledgments

The authors thank the Natural Sciences and Engineering Research Council Discovery grant program as well as the Canada Research Chairs program for funding. In addition, the authors thank the Canada Foundation for Innovation and the Nova Scotia Research and Innovation Trust for infrastructure support. G. St. Marie acknowledges receipt of a Dean of Science Summer Research Award and O. Clarke acknowledges financial support from the Faculty of Graduate Studies and Research. We also thank Dr. Xiang Yang for his technical support with the SEM-EDX instrumentation.

References

1. T. Vo-Dinh, Y. Liu, A. M. Fales, H. Ngo, H. Wang, J. K. Register, H. Yuan, S. J. Norton, and G. D. Griffin, *Wiley Interdisciplinary Reviews-Nanomedicine and Nanobiotechnology*, **7**, 17 (2015).
2. S. Schluecker, *Chemphyschem*, **10**, 1344 (2009).
3. K. L. Wustholz, C. L. Brosseau, F. Casadio, and R. P. Van Duyne, *Phys. Chem. Chem. Phys.*, **11**, 7350 (2009).
4. J. Y. Roh, M. K. Matecki, S. A. Svoboda, and K. L. Wustholz, *Anal. Chem.*, **88**, 2028 (2016).
5. R. A. Alvarez-Puebla, D. S. dos Santos Jr., and R. F. Aroca, *Analyst*, **132**, 1210 (2007).
6. A. J. Pereira, J. P. Gomes, G. F. Lenz, R. Schneider, J. A. Chaker, P. E Narciso de Souza, and J. F. Felix, *J. Phys. Chem.*, **120**, 12265 (2016).
7. Y. Zhao and C. Burda, *Energy & Environmental Science*, **5**, 5564 (2012).
8. G. H. Chan, J. Zhao, E. M. Hicks, G. C. Schatz, and R. P. Van Duyne, *Nano Lett.*, **7**, 1947 (2007).
9. V. E. Ferry, J. N. Munday, and H. A. Atwater, *Adv. Mater.*, **22**, 4794 (2010).
10. M. Rycenga, C. M. Cobley, J. Zeng, W. Li, C. H. Moran, Q. Zhang, D. Qin, and Y. Xia, *Chem. Rev.*, **111**, 3669 (2011).
11. L. Chen, J. Yu, T. Fujita, and M. Chen, *Adv. Funct. Mater.*, **19**, 1221 (2009).
12. V. C. Bassetto, A. E. Russell, L. T. Kubota, and P. N. Bartlett, *Electrochim. Acta*, **144**, 400 (2014).
13. H. Yang, S. He, and H. Tuan, *Langmuir*, **30**, 602 (2014).
14. P. Lu, J. Dong, and N. Toshima, *Langmuir*, **15**, 7980 (1999).
15. E. Giorgetti, P. Marsili, P. Canton, M. Muniz-Miranda, S. Caporali, and F. Giammanco, *J. Nanopart. Res.*, **15**, 1360 (2013).
16. K. Chen, X. Zhang, Y. Zhang, D. Y. Lei, H. Li, T. Williams, and D. R. MacFarlane, *Adv. Mater. Int.*, **3**, 1600115 (2016).
17. K. Chang and H. Chung, *RSC Advances*, **6**, 75943 (2016).
18. L. Zhao, J. Blackburn, and C. L. Brosseau, *Anal. Chem.*, **87**, 441 (2015) A. M. Robinson, S. G. Harroun, J. Bergman, and C. L. Brosseau. *Anal. Chem.*, **84**, 1760 (2012)
19. C. A. Schneider, W. S. Rasband, and K. W. Eliceiri, *Nat. Methods*, **9**, 671 (2012).
20. G-Z. Yuan, C-F. Hsia, Z-W. Lin, C. Chiang, Y-W. Chiang, and M. H. Huang, *Chem. Eur. J.* **22**, 12548 (2016).
21. D. A. Skoog, D. M. West, F. J. Holder, and S. R. Crouch, *Eds.; Fundamentals of Analytical Chemistry 8th ed., Brook/ Cole Cengage Learning: United States of America*, (2004).
22. D. K. Sharma, A. Ott, A. P. O'Mullane, and S. K. Bhargava, *Colloids Surf. Physicochem. Eng. Aspects*, **386**, 98 (2011).
23. S. Wang, L. Xu, Y. Wen, H. Du, S. Wang, and X. Zhang, *Nanoscale*, **5**, 4284 (2013).
24. X. Li, M. Li, P. Cui, X. Zhao, T. Gu, H. Yu, Y. Jiang, and D. Song, *Crystengcomm*, **16**, 3834 (2014).
25. C. Zhang, Y. Lu, B. Zhao, Y. Hao, and Y. Liu, *Appl. Surf. Sci.*, **377**, 167 (2016).
26. J. Bian, Z. Chen, Z. Li, F. Yang, H. He, J. Wang, J. Z. Y. Tan, J. Zeng, R. Peng, X. Zhang, and G. Han, *Appl. Surf. Sci.*, **258**, 6632 (2012).
27. J. Bian, S. Shu, J. Li, C. Huang, Y. Y. Li, and R. Zhang, *Appl. Surf. Sci.*, **333**, 126 (2015).
28. J. Fang, Y. Yi, B. Ding, and X. Song, *Appl. Phys. Lett.*, **92**, **131115**, (2008).
29. X. Ke, B. Lu, J. Hao, J. Zhang, H. Qiao, Z. Zhang, C. Xing, W. Yang, B. Zhang, and J. Tang, *Chemphyschem*, **13**, 3786 (2012).
30. D. Li, J. Liu, H. Wang, C. J. Barrow, and W. Yang, *Chem. Comm.*, **52**, 10968 (2016).
31. A. M. Robinson, L. Zhao, M. Y. Shah Alam, P. Bhandari, S. G. Harroun, D. Dendukuri, J. Blackburn, and C. L. Brosseau, *Analyst*, **140**, 779 (2015).
32. A. D. Zamkovets, A. N. Ponyavina, and L. V. Baran. *J. Opt. Technol.*, **77**(7), 456 (2010).
33. A. K. Sharma and G. J. Mohr. *J. Phys. D: Appl. Phys.* **41**, 055106 (2008).
34. A. Zamkovets, A. Panyavina, and L. Baran. *J. Opt. Technol.* **77**, 456 (2010).
35. Y. Fang, Y. Li, H. Xu, and M. Sun, *Langmuir*, **26**, 7737 (2010).
36. M. Sun and H. Xu. *Small*, **8**(18), 2777 (2012).
37. M. Osawa, N. Matsuda, Y. Katsumasa, and I. Uchida. *J. Phys. Chem.* **98**, 12702 (1994).